How ultra-narrow gap symmetries control plasmonic nanocavity modes: from cubes to spheres

Rohit Chikkaraddy[†], Xuezhi Zheng[‡], Felix Benz[†], Laura J. Brooks[†], Bart de Nijs[†], Cloudy Carnegie[†], Marie-Elena Kleemann[†], Jan Mertens[†], Richard W. Bowman, Guy A. E. Vandenbosch[‡], Victor V. Moshchalkov[§], and Jeremy J. Baumberg[†].

[†] NanoPhotonics Centre, Cavendish Laboratory, Department of Physics, JJ Thompson Avenue, University of Cambridge, Cambridge, CB3 0HE, United Kingdom

[‡] Department of Electrical Engineering (ESAT-TELEMIC), KU Leuven, Kasteelpark Arenberg 10, BUS 2444, 3001 Leuven, Belgium

[§] Laboratory of Solid State Physics and Magnetism, KU Leuven Celestijnenlaan 200D, Heverlee, B-3001, Belgium

KEYWORDS: Plasmonics, Nanocavities, Patch antennas, Purcell factor, Metasurfaces, Strong coupling and SERS.

ABSTRACT.

Plasmonic nanocavities with sub-5nm gaps between nanoparticles support multiple resonances possessing ultra-high field confinement and enhancements. Here we systematically compare the two fundamentally different resonant gap modes: transverse waveguide (s) and antenna modes (l) which, despite both tightly confining light within the gap, have completely different near-field and far-field radiation patterns. By varying the gap size, both experimentally and theoretically, we show how changing the nanoparticle shape from sphere to cube alters coupling of s and l modes resulting in strongly hybridized (j) modes. Through rigorous group representation analysis we identify their composition and coupling. This systematic analysis shows modes with optical field perpendicular to the gap are best to probe the optical properties of cavity-bound emitters, such as single molecules.

Effective ways to enhance, confine, couple, and utilize light down to the single-emitter level have been central questions of nanophotonics[1–3]. Plasmonic nanocavities made of noble metallic nanostructures have played an important role in addressing this, using collective charge oscillations of surface plasmon polaritons[4,5]. Surface plasmons on closely-spaced multiple nanostructures can hybridize with each other to create trapped modes within their gap[6]. Such nano-gaps are used to probe optical properties of single-molecules such as their Raman scattering[7–9], non-linear effects[10], chiral activity[11], or rate of emission[12]. However, resonant enhancements depend strongly on the morphology of the gap, especially when gaps

are sub-5nm.[13–20] This results in a complex set of multiple modes influencing the optical properties at a given wavelength of interest. While a number of geometries have been reported in the literature[18,21–29], it remains completely unclear which are optimal for coupling light into emitters within these nano-cavities. To tackle this, parameters such as the local field strength, far-field cross-sections, losses due to damping, and spatial charge distributions across the geometry need to carefully analyzed. To understand then how the individual modes influence these parameters, a suitable decomposition technique is required. Here we exemplify these issues by considering two extreme dimer nano-architectures based on cubes with sharp edges, and spheres with smooth surfaces. We develop a theoretical framework that provides ideal decomposition of the modes, which is used to quantify their different Purcell factors.

Theoretically, plasmonic dimers consisting of two closely-spaced noble-metal nanoparticles can provide field enhancements and confinement that push beyond classical assumptions[30–32]. In practice, precise and reliable top-down fabrication of such nanoscale gaps is extremely challenging. By contrast, bottom-up approaches (for instance using self-assembled monolayers) allow very precise spacing between nanoparticles and flat metal films coated with insulating[33,34] or conductive layers[35]. Charge oscillations in such nanoparticles deposited on top of nm-thick spacer layers then couple to image charges in the flat film[36,37], providing equivalent enhancements and confinement to the plasmonic dimer system. This is thus the plasmonic nanocavity system of choice due to its remarkable precision and reproducibility[38–40]. The tightly confined nanocavity modes couple into the far-field by mixing with antenna modes ($l_{1,2,..}$) of the system, which radiate efficiently because their dipolar charge is distributed over the whole nano-construct. Effective in- and out-coupling thus depends on matching symmetries of antenna and nanocavity modes.

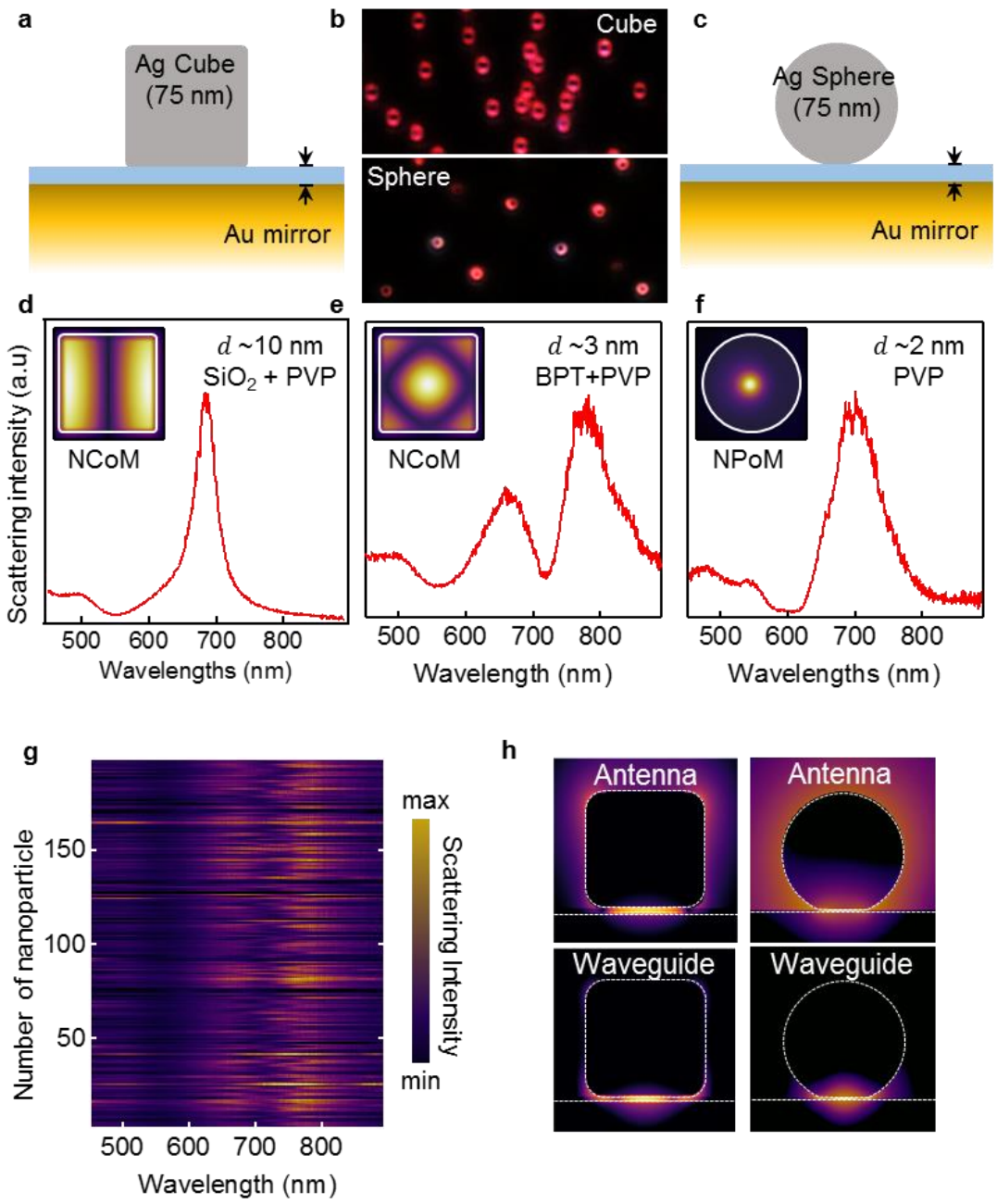

Figure 1. Nanocube vs nanosphere image-dimers. **(a)** Schematic of Ag nanocube with 75 nm edge length placed on template-stripped Au with sub-5 nm molecular gaps. **(b)** Optical dark-field images of (top) nanocubes and (bottom) nanospheres placed on Au mirror with BPT and PVP spacers respectively. **(c)** Schematic of NPoM. **(d-f)** Scattering spectra from (d,e) 75 nm nanocubes with (d) d=10 nm SiO_2 spacer, (e) 3 nm BPT spacer, and (f) nanosphere with 2 nm PVP spacer. Inset color maps show normalized near-field intensity at the resonance wavelength, taken at the middle of gap; white lines indicate nanostructure edges. **(g)** Scattering from >200 nanoparticles of 75 nm Ag PVP-coated nanocubes placed on Au mirror with BPT spacer. **(h)** Near-field distributions of antenna (l_1) and waveguide (s_{02}) modes for (left) cube NCoM and (right) sphere NPoM (see text).

Here we systematically compare the near- and far-field optics of film-coupled nanocubes (termed nanocube-on-mirror or NCoM) and nanospheres (nanoparticle-on-mirror, NPoM) for sub-5 nm gaps (Fig. 1a-c). Recent studies show that both these systems exhibit extreme nano-optics such as ultrafast photon emission from cubes NCoMs[41] and strong-coupling from spherical NPoMs in the single-emitter regime[42]. Two fundamental parameters of a cavity describe how well it enhances light-matter interactions. The quality ($Q = \omega_c/\kappa$) factor describes how long a photon can be confined within the cavity and is calculated from the spectral width κ and the resonant frequency of the cavity ω_c. The second parameter is the effective field localization V_{eff}, which characterizes the confinement of the cavity mode. Different power law scalings of Q and V_{eff} influence different optical phenomena and, as we show, are influenced by nanoparticle shape.

The fundamental (or lowest order) cavity resonance of the cube NCoM structure (seen in the near-IR with larger gaps, Figs.1d,S1a) has $Q\sim25$ with strong field enhancements near the nanocube edges (inset Fig.1d). By contrast, spherical NPoMs have highest field confinement at the center with broader resonances ($Q\sim15$, Fig. 1f). For nanogaps below 5 nm the optical dark-field images of NCoMs and NPoMs both exhibit doughnut spatial profiles (Fig. 1b), which are characteristic of vertical radiating dipoles, confirming the coupling to image charges in the metal film. However, spectra of this collected scattered light exhibit completely different resonance features (Fig. 1e,f). For such small gaps, the question of which resonance is most effective for molecular nano-optics is the focus of this work.

Because several resonant mixed modes can contribute to Q and V_{eff} at any given wavelength, it is not easy to understand their dependences without decomposing the observed peaks into fundamental modes. We thus first show how to deconvolve the observed composite plasmonic modes of this nanoparticle-on-mirror geometry (focusing on the cube initially, as [Ref. 20] describes modes of a sphere) and analyze how these modes interfere in the near-field and far-field response using a symmetry-based eigenmode decomposition. We can track these fundamental modes while tuning the gap size and obtain the deconvolved charge distributions for the dominant two lowest modes of cube NCoMs. We then show how these two modes evolve on transforming the cube NCoM into the sphere NPoM. We find different types of modes are involved, with waveguide modes closely confined to the gap and antenna modes with significant amplitude on the top of the nanoparticles (Fig.1h). Finally, once we have pure charge distributions for these fundamental modes we come back to the figures of merit for different modes and quantify which system is most effective for coupling to single-molecules.

Characterization of nanocavity modes in cube NCoM: To characterize the resonances of cube NCoMs with gaps below 5 nm, we fabricate samples with self-assembled monolayers of

biphenyl-4-thiol (BPT) on template-stripped gold and then assemble silver nanocubes (edge length 75 nm) on top, resulting in NCoMs with gaps of 2-3 nm (note that nanocubes are coated with 1-1.5 nm thick poly(vinylpyrrolidinone) (PVP) on the surface). Dark-field scattering spectra from many such NCoMs (Fig. 1g) consistently exhibit two optical resonances, with average peak positions around 650 nm and 780 nm. The small variation in peak position from nanoparticle to nanoparticle is associated with differences in nanoparticle size, PVP coverage, and their edge rounding (see below).

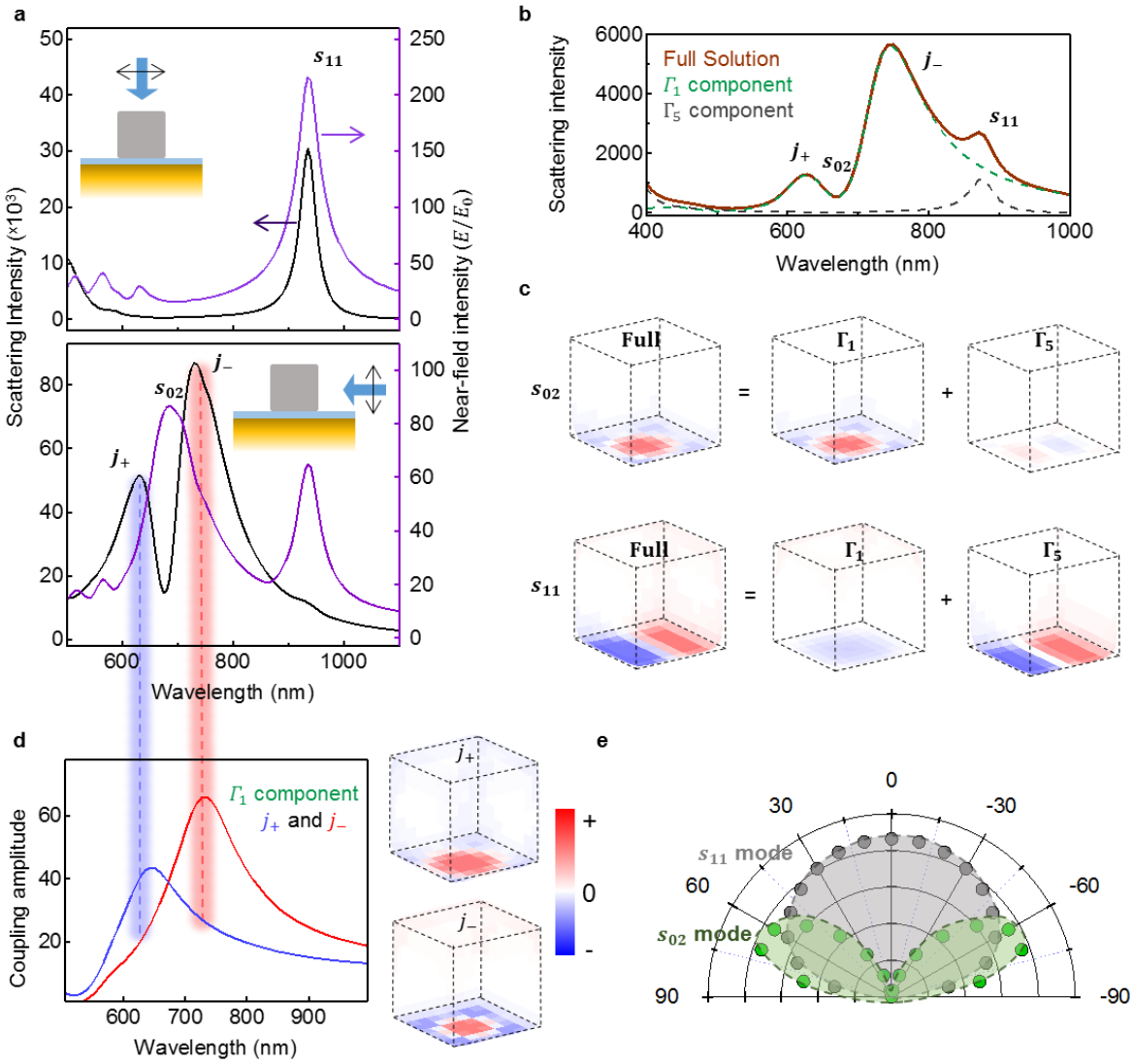

Figure 2. Simulated nanocavity resonances of nanocube with 3 nm gap. **(a)** FDTD scattering (black) and near-field spectra (purple) for 75 nm Ag cube on Au mirror with 3 nm gap of n=1.4, under normal (top) and perpendicular (bottom) illumination (insets). **(b)** BEM scattering full solution (orange) at 55° incidence, with projections from 1st (dashed green) and 5th (dashed gray) irreducible representations. **(c)** Charge distributions and decompositions at λ_s peaks in (b). **(d)** Amplitudes of $j_\pm$ modes and charge distributions to Γ_1. **(e)** Angle dependent far-field coupling pattern for s_{02}, s_{11} modes.

Better insight is obtained using 3D finite-difference time-domain (FDTD) simulations (Fig. 2a). For normal illumination with electric field polarized parallel to the metal surface, only one resonance mode at longer wavelength (600-1200 nm) is observed in the far-field scattering spectrum (scattering intensity integrated over all directions). The same resonance mode is observed in the near-field and labelled s_{11} because its field profile shows charge oscillations between each edge of the nanocube indicating a transverse waveguide feature[43] (Fig. 1d inset). The indices indicate the number of intensity maxima along radial and azimuthal angles along the bottom facet of nanostructure[20] (Fig. S1b). Illumination almost parallel to the metal film with electric field polarized perpendicular to the metal surface shows a completely different spectrum. The near-field still shows s_{11} but also a new resonance labelled s_{02} is observed at 690 nm. Unlike s_{11} which has a nodal line across the center of the nanocube, the s_{02} mode is maximum at the center and each corner of the nanocube (Fig. 1e, inset). In far-field however, the strong scattering resonance at s_{11} (950 nm) is absent and two new resonances labelled j_+ and j_- appear at 610 and 750 nm (which we will discuss in detail later but come from mixing s_{02} and l_1), with lineshapes that are not Lorentzian. Similar modes are also observed in cropped spheres with NPoM geometry[20,44] where strong mixing is found between l_1 and s_{02} modes.

Symmetry based decomposition of nanocavity modes: The origin of the resonances in near- and far-field in Fig. 2a can be better understood through group representation theory analysis[45–49]. The symmetry operations of the NCoM structure form the C_{4v} group which has five irreducible representations (*irrep,* Γ). For each Γ_i, a projection operator can be constructed (details are provided in section SI2 and Fig. S2). The application of all projection operators to a function results in *basis functions* that belong to different Γ_i. More importantly, the obtained basis functions are orthogonal to each other in an inner product sense. Therefore, the optical response from a BEM solver[45–50] including the surface charge, surface currents, near-, and far-fields of the NCoM can be decomposed according to Γ_i. For a given incident field, the full solution of the surface charge can thus be decomposed into surface charge basis functions (Fig. 2b,c) belonging to the first (Γ_1) and fifth (Γ_5) irreps. Inspecting the charge contributions from $\Gamma_{i=1..5}$ (Fig. S3) clearly shows that Γ_{2-4} do not contribute significantly to the total field in the gap. The surface-charge basis functions act as sources inducing the near- as well as the far-field. When the scattering cross section is evaluated, due to their orthogonality, no interference between Γ_1 and Γ_5 is observed. This immediately allows an additive decomposition of the scattering cross section, as easily confirmed by comparing the orange curve (Fig. 2b, full solution) with the dashed green and gray curves (σ_S due to Γ_1 and Γ_5 respectively) which shows they are not coupled or interfering. The scattering cross section associated with Γ_5 has a prominent resonance around 880 nm and weaker resonances at and below 400 nm (Fig. 2b) which correspond to higher order s_{ij} modes. The narrow s_{11} mode (880 nm) is weak in the region of the $j_\pm$ modes (which are associated with Γ_1, dashed green).

Corresponding features are seen in the near-field charge distributions (Figs. 2c, S3): Γ_1 contributes to two resonances labelled $j_\pm$ (627,750 nm), with similar charge distributions maximised at the center of the bottom cube face. These modes come from the mixing of s_{02} and l_1 (which are deconvoluted in Fig.1h to show the underlying basis states), and give constructive interference in the near-field that leads to a near-field maximum at 665 nm (Fig.2a lower). The amplitude of these $j_\pm$ modes shows overlapping spectral components (Fig.2d), however there is a π shift between their emission phases (Fig.S4) which means they destructively interfere in the far-field. At the wavelength of the central dip between the $j_\pm$ resonances, their near-fields within the gap constructively add while in the far-field they cancel out. This can also be seen from their opposite charge on the top surface of the cube (Fig. 2d, right),[51] thus giving their asymmetric line shapes. It is important to note that when $j_\pm$ couple to molecules, it is through their local near-field in the gap whereas far-field radiation of these modes is driven by the oscillating charge on the top surface of the nanocube.

Even though s_{11} and s_{02} modes are projections of different Γ_i, their near-fields both have major contributions from $\boldsymbol{E}_z$ components. Intrigued by this aspect we checked the angle-dependent scattering cross-sections (Figs. 2e, S5, section SI5) and find that s_{11} modes have maximum coupling efficiency for $\boldsymbol{k}$ normal to the surface (horizontal dipoles) while for s_{02} modes coupling is maximized for $\boldsymbol{k}$ incident at 60 degrees to the film normal (vertical dipoles). It thus turns out that symmetry breaking from the nanoparticle-on-mirror geometry (compared to a nanoparticle dimer) allows a horizontal input field to partially couple to a vertical quadrupole with strong $\boldsymbol{E}_z$.[38,52]

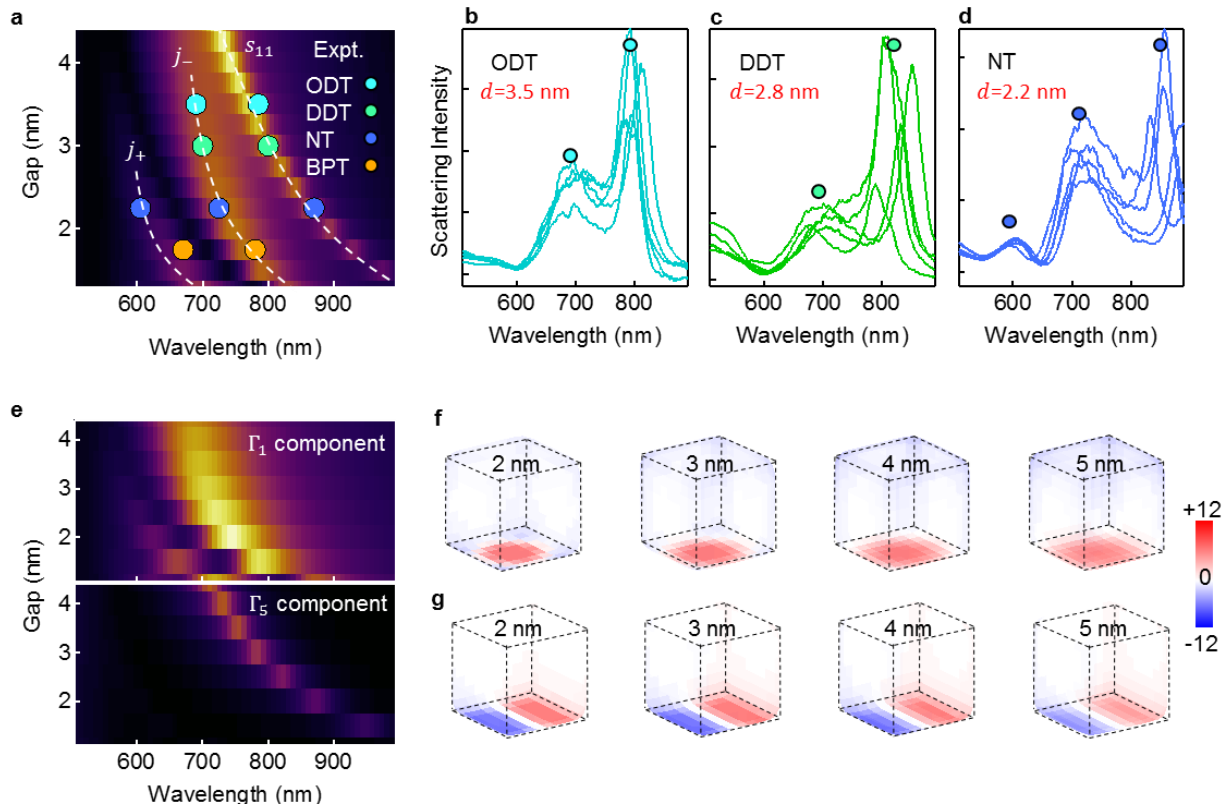

Figure 3. Evolution of nanocavity modes with gap size. **(a)** Experimental resonance positions (colored points) of s_{11} and $j_{\pm}$ modes for different molecular spacers in addition to PVP coating (see text, dotted lines are guides to eye). Background color map shows calculated spectra with gap size. **(b-d)** Scattering spectra obtained for different molecular spacers of d (b) 3.5 nm, (c) 2.8 nm, and (d) 2.2 nm thickness. Peak positions are marked by color-coded dots as in (a). **(e)** Evolution of scattering cross sections from projections of Γ_1 and Γ_5 *vs* gap size. **(f, g)** Evolution of charge confinement *vs* gap size (d as marked) for (f) Γ_1 and (g) Γ_5.

Variation of gap size effecting the nanocavity modes: To track the formation and evolution of these hybrid $j_{\pm}$ modes, the spacer thickness (d) is tuned by using different aliphatic self-assembled monolayers. Molecular monolayers of 1-octadecanethiol, 1-dodecanethiol and 1-nonanethiol have decreasing chain lengths (18, 12, and 9 carbon atoms respectively) resulting in gaps of 3.5, 2.8 and 2.2 nm (as previously determined[53]) including the layer of PVP around the nanocubes. Both experimentally and numerically the s_{11} scattered mode is seen to rapidly shift from 800 nm to 900 nm for a small reduction in gap from 3.5 nm to 2.2 nm (Fig. 3a-d). In these experiments BPT molecular spacers have a larger refractive index than aliphatic monolayers so the s_{11}mode is shifted further into the infrared and cannot be observed in our optical dark-field setup.

This s_{11} mode scattering strength weakens as the gap decreases (Fig. 3a), which makes it hard to couple into this mode at smaller gaps, while limiting the field confinement essential for extreme nano-optics. On the other hand, the $j_{\pm}$ resonances become prominent at smaller gaps, which correlates with their increasing proximity to the l_1 mode (as seen for NPoMs of equivalent volume, Fig. S6). The coupling of the $j_{\pm}$ modes intensifies and exhibits a systematic red-shift as the gap size decreases (Fig. S8), which is in good agreement with the observed trend in scattering cross sections shown in Fig. 3a-d. The surface charge distribution also varies with gap size (Fig. 3f). As the gap size reduces, the bottom surface charges concentrate more to the center, attributed to the increased attraction exerted by the image charges in the underlying mirror.

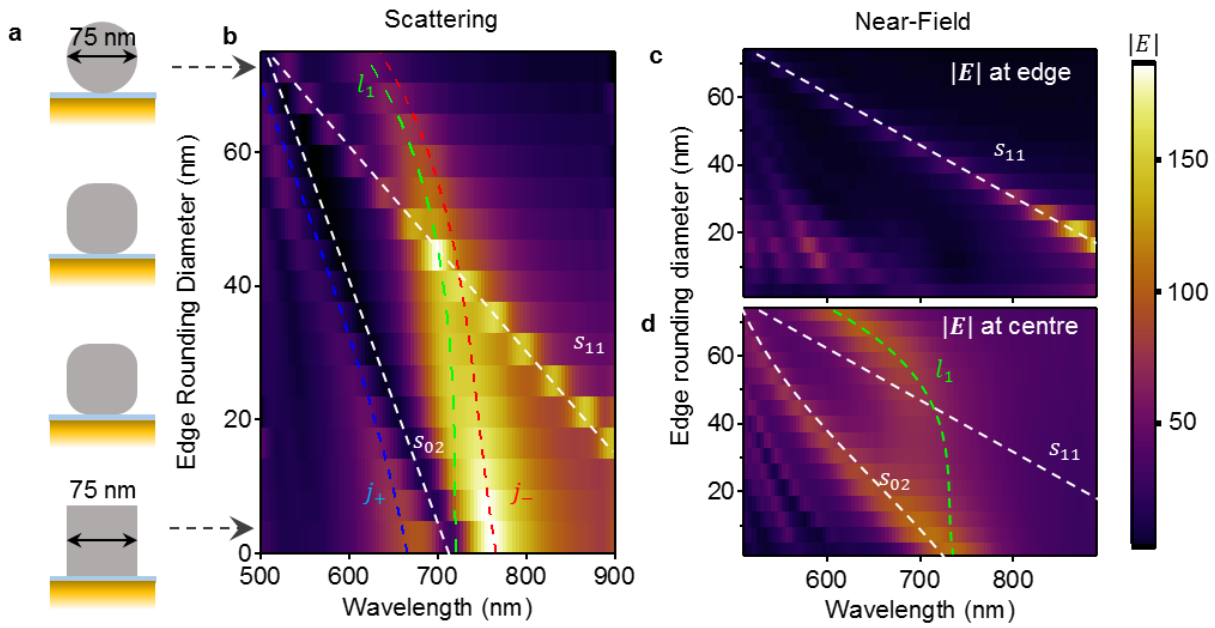

Figure 4. Evolution from nanocube to nanosphere with 3 nm gap. **(a)** Schematic of smoothly transforming nanocube of edge length 75 nm into nanosphere of 75 nm diameter by tuning the edge rounding parameter. **(b)** Simulated 3D FDTD scattering spectra obtained for nanostructures defined in (a). Resonance wavelengths of modes vary due to change in volume (l_1, green line) and edge length (s_{ij}, white lines) of nanostructure. Calculated resonance position of j_+ and j_- due to mixing between l_1 and s_{02} modes shown as red/blue dashed lines. **(c,d)** Near-field intensities vs λ, (c) at edge, and (d) at center of lower gap facet, resonant modes color coded as (b).

Tuning the shape of nanocavity from cube NCoM to sphere NPoM: Clear identification of the s, l and j modes is obtained from simulations in which NCoMs are gradually transformed into NPoMs by progressively rounding the edges of the nanocube (Fig. 4a). Increasing the nanocube edge roundness linearly blue-shifts the s_{11} NCoM mode as the facet diameter decreases (Fig.4b), becoming no longer the ground state for the NPoM after 60% rounding. Discrimination of the modes by symmetry is achieved by monitoring the near-field spectra at

the edge (s_{11}) and centre (s_{02}, l_1) of the nanostructure (Fig. 4c,d). The l_1 mode of an equivalent sphere NPoM which is given the same total volume as this progressively rounded cube (Fig.2d, dashed green) almost exactly tracks the resonance observed in the near-field at the facet centre. The predicted position of $j_\pm$ modes (red/blue dotted lines, Fig. 4b) is calculated from the frequencies of l_1 and s_{02} from near-field (Fig.4d) with a coupling strength of 250 meV obtained for this scenario.

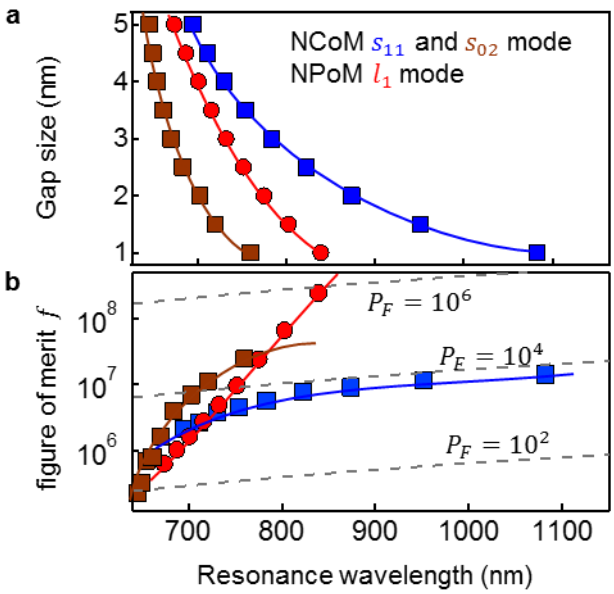

Figure 5. Comparing molecular-coupling figure of merit for cube NCoM and sphere NPoM of same volumes. **(a)** Resonance frequency of NCoM modes (square dots) and NPoM mode (circular dots) with gap size. **(b)** Figure of merit for modes (color-coded as in a), dotted gray lines indicate Purcell factors P_F.

Figure of merit: The molecular-coupling efficiencies of NPoM and NCoM systems can now be compared, being careful to use the same particle volume for each (Fig. 5). We first note that for small gaps, the s_{11} mode in cubes is always at much longer wavelengths than the s_{02} modes making it awkward to utilize in coupling with electronic resonances in the visible and near-IR (high-oscillator-strength electronic transitions of molecules or semiconductors are hard to tune into the IR as they come from larger less-localized electronic states). The s_{02} modes support near-field enhancements that exceed the s_{11} mode for gaps d<2.2nm, and slightly exceed those found for spherical NPoMs. Although for larger gaps (d>2.2nm) the cube NCoM produces higher field enhancements from the s_{11} mode, this is always at longer wavelengths (beyond 720nm) and for the same spectral resonance position, the s_{02} is always preferred.

Of most importance however is the mode volume as well as the field enhancement. The effective mode volume for s_{11} and s_{02} from the cube NCoM is considerably larger than the l_1 mode of sphere NPoMs (Fig. S10). We define a suitable figure of merit comparing these modes that is proportional to the Rabi coupling strength and thus involves both near-field enhancement and mode volume, as

$$f = \{(E^2/E_0^2)/(A_{\text{eff}}/A_\lambda)\} \quad (1)$$

where the effective lateral mode area A_{eff} for the l_1 mode is πRd and for the s_{11}, s_{02} modes is $\sim L^2/4$ where R is the radius of nanosphere and L is the edge length of the nanocube. The normalization is to $A_\lambda = (\lambda/n)^2$ where λ/n is the wavelength of the resonance in the gap medium. For gaps d > 4 nm, s_{11} has larger f values than the other two modes with Purcell factor ($\propto Q/V$) up to 7×10^3, however as the gap becomes smaller, the coupling f saturates for cube modes s_{11} and s_{02} (Fig. 5b). In contrast, the l_1 mode dominates for gaps <2.2nm with large f values and Purcell factors exceeding 10^6. For this reason, the desirable extreme nano-optics regime of coupling to single emitters will always favour the sphere NPoM with vertical dipole orientation, rather than the s_{11} mode in cubes. We note that some degree of faceting is always inevitable, hence in practice mixed s_{02} - l_1 modes will be obtained. However these conclusions hold in practical experiments where neither extreme geometry is feasible, since nanospheres are faceted and nanocubes have rounded edges.

In summary, we have experimentally and theoretically compared the effect of nanoparticle shape for the prototypical coupling between plasmonic components. For gaps of a few nanometers, we find that optical coupling to emitters is favoured for modes with plasmonic fields perpendicular to the gap, although input coupling is easier for the geometry where the plasmonic fields are parallel to the gap. This analysis should be useful to design optimal experiments and explore the extreme nano-optics domain opened up.

ASSOCIATED CONTENT

Supporting Information. Details about Eigen mode decomposition and group symmetry, dark-field scattering spectrum, experimental radiation pattern, coupling strengths and comparing l_1, s_{02} and s_{11} nanocavity modes. This material is available free of charge via the Internet at http://pubs.acs.org." For instructions on what should be included in the Supporting Information, as well as how to prepare this material for publication, refer to the journal's Instructions for Authors.

AUTHOR INFORMATION

Corresponding Author

* Prof Jeremy J Baumberg, jjb12@cam.ac.uk

ACKNOWLEDGMENT

We acknowledge financial support from EPSRC Grants EP/G060649/1, EP/K028510/1, EP/L027151/1, ERC Grant LINASS 320503. R.C. acknowledges support from the Dr. Manmohan Singh scholarship from St. John's College. F.B. acknowledges support from the Winton Programme for the Physics of Sustainability. GAEV, VVM and XZ like to acknowledge the C2 project (C24/15/015) and the PDMK/14/126 project of KU Leuven, the FWO long term stay abroad project grant V405115N, and the Methusalem project funded by the Flemish government.

REFERENCES

(1) Koenderink, A. F.; Alù, A.; Polman, A. Nanophotonics: Shrinking Light-Based Technology. *Science* **2015**, *348*, 516–521.
(2) Pelton, M. Modified Spontaneous Emission in Nanophotonic Structures. *Nat. Photonics* **2015**, *9*, 427–435.
(3) Gramotnev, D. K.; Bozhevolnyi, S. I. Nanofocusing of Electromagnetic Radiation. *Nat. Photonics* **2014**, *8*, 13–22.
(4) Schuller, J. A.; Barnard, E. S.; Cai, W.; Jun, Y. C.; White, J. S.; Brongersma, M. L. Plasmonics for Extreme Light Concentration and Manipulation. *Nat. Mater.* **2010**, *9*, 193–204.
(5) Tame, M. S.; McEnery, K. R.; Özdemir, Ş. K.; Lee, J.; Maier, S. A.; Kim, M. S. Quantum Plasmonics. *Nat. Phys.* **2013**, *9*, 329–340.
(6) Zhu, W.; Esteban, R.; Borisov, A. G.; Baumberg, J. J.; Nordlander, P.; Lezec, H. J.; Aizpurua, J.; Crozier, K. B. Quantum Mechanical Effects in Plasmonic Structures with Subnanometre Gaps. *Nat. Commun.* **2016**, *7*, 11495.
(7) Le Ru, E. C.; Etchegoin, P. G. Single-Molecule Surface-Enhanced Raman Spectroscopy. *Annu. Rev. Phys. Chem.* **2012**, *63*, 65–87.
(8) Kneipp, K.; Wang, Y.; Kneipp, H.; Perelman, L. T.; Itzkan, I.; Dasari, R. R.; Feld, M. S. Single Molecule Detection Using Surface-Enhanced Raman Scattering (SERS). *Phys. Rev. Lett.* **1997**, *78*, 1667–1670.
(9) Nie, S.; Emory, S. R. Probing Single Molecules and Single Nanoparticles by Surface-Enhanced Raman Scattering. *Science* **1997**, *275*, 1102–1106.
(10) Kauranen, M.; Zayats, A. V. Nonlinear Plasmonics. *Nat. Photonics* **2012**, *6*, 737–748.
(11) Valev, V. K.; Baumberg, J. J.; Sibilia, C.; Verbiest, T. Chirality and Chiroptical Effects in Plasmonic Nanostructures: Fundamentals, Recent Progress, and Outlook. *Adv. Mater.* **2013**, *25*, 2517–2534.
(12) Giannini, V.; Fernández-Domínguez, A. I.; Heck, S. C.; Maier, S. A. Plasmonic Nanoantennas: Fundamentals and Their Use in Controlling the Radiative Properties of Nanoemitters. *Chem. Rev.* **2011**, *111*, 3888–3912.
(13) Lee, D.; Yoon, S. Effect of Nanogap Curvature on SERS: A Finite-Difference Time-Domain Study. *J. Phys. Chem. C* **2016**.
(14) Hooshmand, N.; Bordley, J. A.; El-Sayed, M. A. Are Hot Spots between Two Plasmonic Nanocubes of Silver or Gold Formed between Adjacent Corners or Adjacent Facets? A DDA Examination. *J. Phys. Chem. Lett.* **2014**, *5*, 2229–2234.

(15) Nicoletti, O.; de la Peña, F.; Leary, R. K.; Holland, D. J.; Ducati, C.; Midgley, P. A. Three-Dimensional Imaging of Localized Surface Plasmon Resonances of Metal Nanoparticles. *Nature* **2013**, *502*, 80–84.
(16) Zhang, S.; Bao, K.; Halas, N. J.; Xu, H.; Nordlander, P. Substrate-Induced Fano Resonances of a Plasmonic Nanocube: A Route to Increased-Sensitivity Localized Surface Plasmon Resonance Sensors Revealed. *Nano Lett.* **2011**, *11*, 1657–1663.
(17) Bordley, J. A.; Hooshmand, N.; El-Sayed, M. A. The Coupling between Gold or Silver Nanocubes in Their Homo-Dimers: A New Coupling Mechanism at Short Separation Distances. *Nano Lett.* **2015**, *15*, 3391–3397.
(18) Esteban, R.; Aguirregabiria, G.; Borisov, A. G.; Wang, Y. M.; Nordlander, P.; Bryant, G. W.; Aizpurua, J. The Morphology of Narrow Gaps Modifies the Plasmonic Response. *ACS Photonics* **2015**, *2*, 295–305.
(19) Grillet, N.; Manchon, D.; Bertorelle, F.; Bonnet, C.; Broyer, M.; Cottancin, E.; Lermé, J.; Hillenkamp, M.; Pellarin, M. Plasmon Coupling in Silver Nanocube Dimers: Resonance Splitting Induced by Edge Rounding. *ACS Nano* **2011**, *5*, 9450–9462.
(20) Tserkezis, C.; Esteban, R.; Sigle, D. O.; Mertens, J.; Herrmann, L. O.; Baumberg, J. J.; Aizpurua, J. Hybridization of Plasmonic Antenna and Cavity Modes: Extreme Optics of Nanoparticle-on-Mirror Nanogaps. *Phys. Rev. A* **2015**, *92*, 53811.
(21) Duan, H.; Fernández-Domínguez, A. I.; Bosman, M.; Maier, S. A.; Yang, J. K. W. Nanoplasmonics: Classical down to the Nanometer Scale. *Nano Lett.* **2012**, *12*, 1683–1689.
(22) Kern, J.; Großmann, S.; Tarakina, N. V.; Häckel, T.; Emmerling, M.; Kamp, M.; Huang, J.-S.; Biagioni, P.; Prangsma, J. C.; Hecht, B. Atomic-Scale Confinement of Resonant Optical Fields. *Nano Lett.* **2012**, *12*, 5504–5509.
(23) Alivisatos, A. P.; Johnsson, K. P.; Peng, X.; Wilson, T. E.; Loweth, C. J.; Bruchez, M. P.; Schultz, P. G. Organization of "Nanocrystal Molecules" Using DNA. *Nature* **1996**, *382*, 609–611.
(24) Viarbitskaya, S.; Teulle, A.; Marty, R.; Sharma, J.; Girard, C.; Arbouet, A.; Dujardin, E. Tailoring and Imaging the Plasmonic Local Density of States in Crystalline Nanoprisms. *Nat. Mater.* **2013**, *12*, 426–432.
(25) Gao, B.; Arya, G.; Tao, A. R. Self-Orienting Nanocubes for the Assembly of Plasmonic Nanojunctions. *Nat. Nanotechnol.* **2012**, *7*, 433–437.
(26) Aizpurua, J.; Bryant, G. W.; Richter, L. J.; García de Abajo, F. J.; Kelley, B. K.; Mallouk, T. Optical Properties of Coupled Metallic Nanorods for Field-Enhanced Spectroscopy. *Phys. Rev. B* **2005**, *71*, 235420.
(27) Knebl, D.; Hörl, A.; Trügler, A.; Kern, J.; Krenn, J. R.; Puschnig, P.; Hohenester, U. Gap Plasmonics of Silver Nanocube Dimers. *Phys. Rev. B* **2016**, *93*, 81405.
(28) Ghenuche, P.; Cherukulappurath, S.; Taminiau, T. H.; van Hulst, N. F.; Quidant, R. Spectroscopic Mode Mapping of Resonant Plasmon Nanoantennas. *Phys. Rev. Lett.* **2008**, *101*, 116805.
(29) Brintlinger, T.; Herzing, A. A.; Long, J. P.; Vurgaftman, I.; Stroud, R.; Simpkins, B. S. Optical Dark-Field and Electron Energy Loss Imaging and Spectroscopy of Symmetry-Forbidden Modes in Loaded Nanogap Antennas. *ACS Nano* **2015**, *9*, 6222–6232.
(30) Ciracì, C.; Hill, R. T.; Mock, J. J.; Urzhumov, Y.; Fernández-Domínguez, A. I.; Maier, S. A.; Pendry, J. B.; Chilkoti, A.; Smith, D. R. Probing the Ultimate Limits of Plasmonic Enhancement. *Science* **2012**, *337*, 1072–1074.

(31) Khurgin, J. B. Ultimate Limit of Field Confinement by Surface Plasmon Polaritons. *Faraday Discuss.* **2015**, *178*, 109–122.
(32) Savage, K. J.; Hawkeye, M. M.; Esteban, R.; Borisov, A. G.; Aizpurua, J.; Baumberg, J. J. Revealing the Quantum Regime in Tunnelling Plasmonics. *Nature* **2012**, *491*, 574–577.
(33) Benz, F.; Chikkaraddy, R.; Salmon, A.; Ohadi, H.; de Nijs, B.; Mertens, J.; Carnegie, C.; Bowman, R. W.; Baumberg, J. J. SERS of Individual Nanoparticles on a Mirror: Size Does Matter, but so Does Shape. *J. Phys. Chem. Lett.* **2016**, *7*, 2264–2269.
(34) Nijs, B. de; Bowman, R. W.; Herrmann, L. O.; Benz, F.; Barrow, S. J.; Mertens, J.; Sigle, D. O.; Chikkaraddy, R.; Eiden, A.; Ferrari, A.; *et al.* Unfolding the Contents of Sub-Nm Plasmonic Gaps Using Normalising Plasmon Resonance Spectroscopy. *Faraday Discuss.* **2015**, *178*, 185–193.
(35) Benz, F.; Tserkezis, C.; Herrmann, L. O.; de Nijs, B.; Sanders, A.; Sigle, D. O.; Pukenas, L.; Evans, S. D.; Aizpurua, J.; Baumberg, J. J. Nanooptics of Molecular-Shunted Plasmonic Nanojunctions. *Nano Lett.* **2015**, *15*, 669–674.
(36) Aravind, P. K.; Metiu, H. Use of a Perfectly Conducting Sphere to Excite the Plasmon of a Flat Surface. 1. Calculation of the Local Field with Applications to Surface-Enhanced Spectroscopy. *J. Phys. Chem.* **1982**, *86*, 5076–5084.
(37) Aravind, P. K.; Metiu, H. The Effects of the Interaction between Resonances in the Electromagnetic Response of a Sphere-Plane Structure; Applications to Surface Enhanced Spectroscopy. *Surf. Sci.* **1983**, *124*, 506–528.
(38) Moreau, A.; Ciracì, C.; Mock, J. J.; Hill, R. T.; Wang, Q.; Wiley, B. J.; Chilkoti, A.; Smith, D. R. Controlled-Reflectance Surfaces with Film-Coupled Colloidal Nanoantennas. *Nature* **2012**, *492*, 86–89.
(39) Akselrod, G. M.; Huang, J.; Hoang, T. B.; Bowen, P. T.; Su, L.; Smith, D. R.; Mikkelsen, M. H. Large-Area Metasurface Perfect Absorbers from Visible to Near-Infrared. *Adv. Mater.* **2015**, *27*, 8028–8034.
(40) Huang, F.; Drakeley, S.; Millyard, M. G.; Murphy, A.; White, R.; Spigone, E.; Kivioja, J.; Baumberg, J. J. Zero-Reflectance Metafilms for Optimal Plasmonic Sensing. *Adv. Opt. Mater.* **2016**, *4*, 328–335.
(41) Hoang, T. B.; Akselrod, G. M.; Argyropoulos, C.; Huang, J.; Smith, D. R.; Mikkelsen, M. H. Ultrafast Spontaneous Emission Source Using Plasmonic Nanoantennas. *Nat. Commun.* **2015**, *6*.
(42) Chikkaraddy, R.; de Nijs, B.; Benz, F.; Barrow, S. J.; Scherman, O. A.; Rosta, E.; Demetriadou, A.; Fox, P.; Hess, O.; Baumberg, J. J. Single-Molecule Strong Coupling at Room Temperature in Plasmonic Nanocavities. *Nature* **2016**, *535*, 127–130.
(43) Lassiter, J. B.; McGuire, F.; Mock, J. J.; Ciracì, C.; Hill, R. T.; Wiley, B. J.; Chilkoti, A.; Smith, D. R. Plasmonic Waveguide Modes of Film-Coupled Metallic Nanocubes. *Nano Lett.* **2013**, *13*, 5866–5872.
(44) Sigle, D. O.; Mertens, J.; Herrmann, L. O.; Bowman, R. W.; Ithurria, S.; Dubertret, B.; Shi, Y.; Yang, H. Y.; Tserkezis, C.; Aizpurua, J.; *et al.* Monitoring Morphological Changes in 2D Monolayer Semiconductors Using Atom-Thick Plasmonic Nanocavities. *ACS Nano* **2015**, *9*, 825–830.
(45) García de Abajo, F. J.; Howie, A. Retarded Field Calculation of Electron Energy Loss in Inhomogeneous Dielectrics. *Phys. Rev. B* **2002**, *65*, 115418.
(46) Hohenester, U. Simulating Electron Energy Loss Spectroscopy with the MNPBEM Toolbox. *Comput. Phys. Commun.* **2014**, *185*, 1177–1187.

(47) Hohenester, U.; Trügler, A. MNPBEM – A Matlab Toolbox for the Simulation of Plasmonic Nanoparticles. *Comput. Phys. Commun.* **2012**, *183*, 370–381.
(48) Waxenegger, J.; Trügler, A.; Hohenester, U. Plasmonics Simulations with the MNPBEM Toolbox: Consideration of Substrates and Layer Structures. *Comput. Phys. Commun.* **2015**, *193*, 138–150.
(49) Vandenbosch, G. A. E.; Capelle, A. R. V. de. Mixed-Potential Integral Expression Formulation of the Electric Field in a Stratified Dielectric Medium-Application to the Case of a Probe Current Source. *IEEE Trans. Antennas Propag.* **1992**, *40*, 806–817.
(50) Zheng, X.; Verellen, N.; Vercruysse, D.; Volskiy, V.; Dorpe, P. V.; Vandenbosch, G. A. E.; Moshchalkov, V. On the Use of Group Theory in Understanding the Optical Response of a Nanoantenna. *IEEE Trans. Antennas Propag.* **2015**, *63*, 1589–1602.
(51) Lombardi, A.; Demetriadou, A.; Weller, L.; Andrae, P.; Benz, F.; Chikkaraddy, R.; Aizpurua, J.; Baumberg, J. J. Anomalous Spectral Shift of Near- and Far-Field Plasmonic Resonances in Nanogaps. *ACS Photonics* **2016**, *3*, 471–477.
(52) Kleemann, M.-E.; Mertens, J.; Zheng, X.; Cormier, S.; Turek, V.; Benz, F.; Chikkaraddy, R.; Deacon, W.; Lombardi, A.; Moshchalkov, V. V.; *et al.* Revealing Nanostructures through Plasmon Polarimetry. *ACS Nano* **2017**, *11*, 850–855.
(53) Benz, F.; de Nijs, B.; Tserkezis, C.; Chikkaraddy, R.; Sigle, D. O.; Pukenas, L.; Evans, S. D.; Aizpurua, J.; Baumberg, J. J. Generalized Circuit Model for Coupled Plasmonic Systems. *Opt. Express* **2015**, *23*, 33255.

For Table of Contents Use Only

How ultra-narrow gap symmetries control plasmonic nanocavity modes: from cubes to spheres

Rohit Chikkaraddy[†], Xuezhi Zheng[‡], Felix Benz[†], Laura J. Brooks[†], Bart de Nijs[†], Cloudy Carnegie[†], Marie-Elena Kleemann[†], Jan Mertens[†], Richard W. Bowman, Guy A. E. Vandenbosch[‡], Victor V. Moshchalkov[§], and Jeremy J. Baumberg[†].

[†] NanoPhotonics Centre, Cavendish Laboratory, Department of Physics, JJ Thompson Avenue, University of Cambridge, Cambridge, CB3 0HE, United Kingdom

[‡] Department of Electrical Engineering (ESAT-TELEMIC), KU Leuven, Kasteelpark Arenberg 10, BUS 2444, 3001 Leuven, Belgium

[§] Laboratory of Solid State Physics and Magnetism, KU Leuven Celestijnenlaan 200D, Heverlee, B-3001, Belgium